Influence of Substrate, Additives, and Pulse Parameters on Electrodeposition of Gold Nanoparticles from Potassium Dicyanoaurate

PARISA VAHDATKHAH and SAYED KHATIBOLESLAM SADRNEZHAAD

Gold nanoparticles (AuNPs) of less than 50 nm diameter were electrodeposited from cyanide solution by pulsating electric current on modified copper and indium tin oxide (ITO) films coated on glass. Morphology, size, and composition of the deposited AuNPs were studied by X-ray photoelectron spectroscopy, atomic force microscopy, and field emission scanning electron microscopy. Effects of peak current density, pulse frequency, potassium iodide and cysteine on grain size, and morphology of the AuNPs were determined. Experiments showed that cathode current efficiency increases with the pulse frequency and the iodide ion. Size of the AuNPs increased with the current density. The number of nucleation sites was larger on ITO than on Cu layer; while the average diameter of the crystallites on ITO was smaller than on Cu layer.

DOI: 10.1007/s11663-015-0427-6

I. INTRODUCTION

AuNPs are of much interest due to their superior conductivity, biocompatibility, adjustable optical and electrical behavior, and high catalytic effects.[1,2] Conductive substrates coated with AuNPs are usable in electronic and biochemical sensors and electrodes owing to their excellent electrocatalytic behavior.[2–7] An example is AuNP-ITO which is used for making electrodes.[8] This material has good electrical conductivity, high stability, and capability to promote heterogeneous electron transfer.[2,3,9]

Applications of AuNP-ITO include the electro-oxidation of uric acid, ascorbic acid, dopamine, norepinephrine, epinephrine,[10] and nitric oxide.[11] AuNP-ITO provides a biocompatible matrix for immobilization of hemoglobin (Hb),[12] effective H_2O_2 reduction catalysis with stable reproducibility,[12] myoglobin (Mb) immobilization, and mediator-free H_2O_2 sensor development[13] with promotion of the electrocatalytic activity of three-dimensional monolayer of 3-mercaptopropionic acid (MPA) assembled on AuNP-ITOs,[14] electrochemical response of the hydroquinone and *p*-aminophenol in phosphate buffer solutions[15] and electrochemical measurement of biomolecules such as simultaneous electrochemical determination of guanosine/guanosine-5′-triphosphate, adenosine/adenosine-5′-triphosphate, and dopamine/serotonin.[4,16]

Cu is the most common interconnecting material of the electronic circuits. Gold nanoparticles deposited onto Cu and ITO result in a collection of many useful properties like low electrical resistivity,[17] Cu-to-Cu adhesive bonding,[18] and transparent conductive behavior.[19] These electrodes are therefore usable in many diverse applications.[19]

Several methods have previously been used for attachment of AuNPs onto ITO.[3,7,8] General strategy has been self-assembly of binder molecules onto ITO. This method has been influenced by catalytic property and conductive behavior of the NPs.[8] To overcome this difficulty, seed-mediated growth has been developed.[4,8] This technique has, however, been complex and time-consuming. RF-sputtering[3] and nano-sphere lithography[20] have also been practiced to attach AuNPs onto an ITO substrate.

Another simple, powerful, and cost effective way for attachment of AuNPs onto a substrate layer has been utilization of the electrochemical method.[7,9,21] In previous trials, cyclic voltammetry, potential-sweeping, and potential-step modes have been used.[6,7,9,22] The formation of gold ion complex with cysteine (2-amino-3-mercaptopropionic acid) has, for example, resulted in enhancement of the number of the electrodeposited AuNPs with bumpy, thorny or dendritic shapes.[9,23] Pulsating current can, however, result in smoother, brighter, finer, and less porous Au grains with respect to the direct current.[24]

This paper is to shed some light on the effect of PED parameters (current density and frequency), cysteine ($HO_2CCH(NH_2)CH_2SH$) and potassium iodide (KI) additives and copper and indium tin oxide (ITO) substrate coats on current efficiency, and surface morphology of the gold nanoparticles electrodeposited by pulse current. Effects of pulse condition, additive type and substrate preparation on thickness, porosity, pore size, and morphology of the AuNPs deposited on Cu and ITO layers are meticulously discussed in this paper.

PARISA VAHDATKHAH, Graduate Student, and SAYED KHATIBOLESLAM SADRNEZHAAD, Professor, are with the Department of Materials Science and Engineering, Sharif University of Technology, P.O. Box 11365-9466, Tehran, Iran. Contact email: sadrnezh@sharif.edu

Manuscript submitted August 19, 2013.
Article published online July 14, 2015.

II. EXPERIMENTAL PROCEDURE

The concentrations of the cyanide-based solution and the additives are shown in Table I. Prior to electrodeposition of AuNPs on modified Cu and ITO electrodes, the working cell was washed with nitric acid and distilled water. The Cu electrode substrates were mechanically polished with #3000 emery paper, aqueous slurries of successively finer alumina powders (particle sizes down to 0.3 and 0.05 μm) and with a polishing micro-cloth so that a mirror finish be eventually obtained.

Before each experiment, the electrode was sequentially cleaned in ethanol, distilled water, and activated acidic solution. It was washed in distilled water and acetone and then immediately immersed in the plating solution to allow subsequent electrodeposition. A stainless steel plate was used as anode of the electrodeposition cell. The implanted ITO-coated glass was ultrasonically cleaned in soapy water, distilled water, and acetone for 15 minutes. Table II illustrates the operational conditions of the electrodeposition.

Au concentration was determined by atomic absorption spectrophotometer (GBC Avanta PM, Australia). Chemical composition and electronic structure of the synthesized AuNPs-modified Cu electrodes were studied by X-ray photoelectron spectroscopy (XPS) using Al Kα anode X-ray source (hv = 1486.6 eV) (Space Company, model EA10 plus). The base pressure of the XPS chamber was below 1×10^{-9} torr and a concentric hemispherical analyzer was employed to measure energy of the emitted electrons from surface of the sample. The XPS peaks were deconvoluted using 75 pct Gaussian +25 pct Lorentzian functional form after a Shirley background subtraction. The energy scale was calibrated by adjusting the carbon peak at 285.00 eV. The concentration for a given element (pct A) was computed by Eq. [1]:

$$\text{pct}A = \frac{\frac{I_A}{S_A}}{\sum \frac{I_A}{S_A}} \times 100, \qquad [1]$$

Table I. Concentrations of the Solution Used in This Study

Constituent	Concentration (g/L)
$KAu(CN)_2$	0.10 (as Au)
$K_4P_2O_7$	1.50
$C_4H_6O_4$	0.50
$C_2H_2O_4$	0.10

where I_A and S_A are the peak area and the sensitivity factor for the element A, respectively. These data are directly provided by the spectrometer software.

Atomic force microscopy (AFM) images were obtained using a Park Scientific model CP-Research instrument (VEECO) with silicon tip of 10 nm radius in the tapping mode. The surface morphology of the Au coatings was characterized by field emission scanning electron microscopy (FE-SEM) (HITACHI model S-4160). Particle sizes and porosity dimensions of the coated substrates were determined by "Image j" and "Clemex Vision" image analysis softwares, respectively.

III. RESULTS AND DISCUSSION

Table III indicates the cathodic current efficiency of Samples 1 to 6. More than twice improvement in current efficiency is observed in Sample 3 which was deposited at frequency of 142.8 Hz. The electric current that pass through the cathode indicates overall reactions occurring in the cell. Metal deposition and hydrogen evolution are commonly taken as the main reactions in the electrochemical cells. Other reactions cause current loss and decreasing of the current efficiency of the process. Current efficiency here is, therefore, defined as the ratio of the current that results in metal deposition to the total current consumed in the cell:

$$\text{Current efficiency(pct)} = \frac{\text{Actual weight deposited}}{\text{Theoretical weight deposited}} \times 100 \qquad [2]$$

Using Faraday's law, the theoretical weight of the deposited layer can be determined:

$$w = \frac{I_{\text{av}} \times t \times \text{atomic weight}}{96{,}500 \times \text{valency}}, \qquad [3]$$

where I_{av} is the average current (duty cycle × peak current) and t is the real time. Theoretical and actual thickness of the depositing layer can also be evaluated from Eq. [4]:

$$T = \frac{w \times 10{,}000}{d \times \text{area}} \text{microns} \qquad [4]$$

A. *XPS Characterization*

Figure 1 illustrates the wide scan XPS spectrum of the AuNPs electrodeposited on Cu electrode.

Table II. Conditions of the Pulse-Current Electrodeposition (Duty Cycle = 30 Pct, Real Time = 1 min)

Sample	Substrate	Total Pulse Time (ms)	On-Time (ms)	Current Density (mA/cm^2)	Current (mA)	Area (cm^2)	Frequency (Hz)	Concentration of Additive (0.05 mM)
1	Cu	20	6	10	10	1	50	cysteine
2	Cu	10	3	10	10	1	100	cysteine
3	Cu	7	2	10	10	1	142.8	cysteine
4	Cu	20	6	5	5	1	50	cysteine
5	Cu	20	6	2.5	5	2	50	cysteine
6	Cu	20	6	10	10	1	50	potassium iodide
7	ITO	20	6	10	10	1	50	cysteine

Table III. Cathodic Current Efficiencies of Samples 1 to 6

Sample	Theoretical Weight (μg)	Weight Electrodeposited (μg)	Current Efficiency (Pct)
1	367.4	96.7	26.32
2	367.4	193.4	52.64
3	367.4	306.2	83.34
4	183.7	80.5	43.84
5	183.7	32.2	17.55
6	367.4	241.7	65.80

Test conditions are given in Table II.

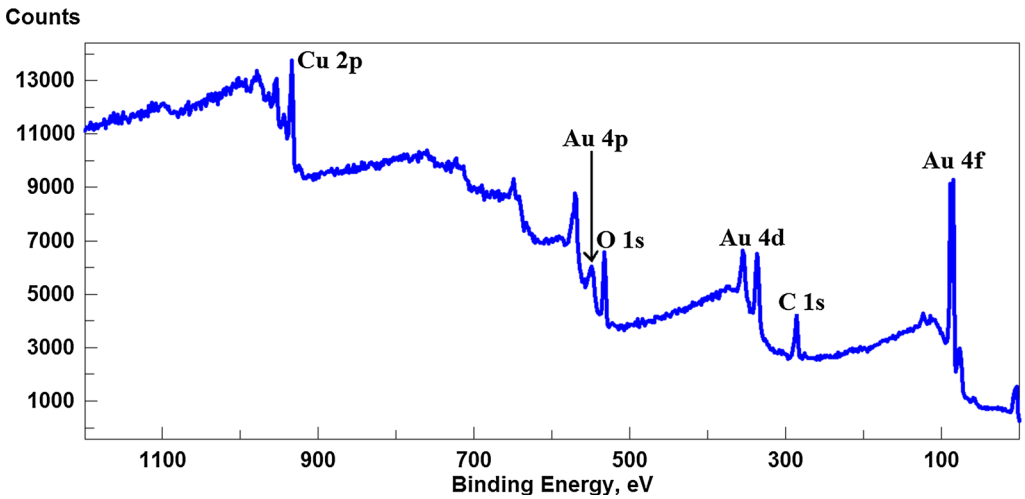

Fig. 1—Wide scan XPS spectrum of AuNPs-modified Cu electrode.

In order to understand the state of gold electrodeposited on Cu electrode, X-ray photoelectron spectra of the deposited layer was recorded for Au 4f of the AuNPs-Cu electrodes (Figure S1a; Supporting Information). No N 1s peak (at 398.5 eV) is observed in the XPS spectra (Figure S1b; Supporting Information), indicating no C-N bond formation on the AuNPs-Cu electrode.

Based on the literatures,[25–27] at low current density and overvoltage, the reduction of the aurocyanide complex proceeds according to the following mechanism:

$$\left[\mathrm{Au(CN)_2}\right]^- \rightarrow \left(\mathrm{AuCN}\right)_{\mathrm{ad}} + \mathrm{CN}^- \qquad [5]$$

$$\left(\mathrm{AuCN}\right)_{\mathrm{ad}} + e \rightarrow \left(\mathrm{Au^0CN}\right)_{\mathrm{ad}}^- \qquad [6]$$

$$\left(\mathrm{Au^0CN}\right)_{\mathrm{ad}}^- \Leftrightarrow \mathrm{Au_{lattice}} + \mathrm{CN}^- \qquad [7]$$

At high current densities and overvoltages, direct reduction of $\left[\mathrm{Au(CN)_2}\right]^-$ occurs without the formation of an adsorbed intermediate:

$$\left[\mathrm{Au(CN)_2}\right]^- + e \rightarrow \mathrm{Au} + 2\mathrm{CN}^- \qquad [8]$$

Previous authors[25] have indicated $\mathrm{CN_{ads}^-}$ and $\mathrm{AuCN_{ads}}$ as the dominant species at smaller currents and $\mathrm{CN_{ads}^-}$ as the dominant species at the higher currents. The XPS results of this study indicate that at 10 mA/cm[2] there is no $\mathrm{AuCN_{ads}}$ while $\mathrm{CN_{ads}^-}$ species are present on the surface. The mechanism of deposition is hence according to Eq. [8]. The XPS peaks of Au $4f_{5/2}$ and Au $4f_{7/2}$ occur at 87.85 and 84.20 eV. These values show respective shifting of 0.15 and 0.20 eV with respect to the known binding energies of bulk metallic gold (87.70 and 84.00 eV).

The XPS result for C 1s is given in S1c (Supporting Information). The carbon peak at 285.00 eV with no C-N contribution (286.00 eV) is observed which is in agreement with results of the previous section. Figure S1d (Supporting Information) shows the XPS spectra of the substrate copper. All Cu $2p_{3/2}$ peaks are composed of 3 peaks deconvolutable to a small peak at about 932.4 eV and two dominant peaks at 932.6 and 933.9 eV. The small peak (at 932.4 eV) corresponds to Cu of Cu(I) oxide. Two dominant peaks (at 932.6 and 933.9 eV) correspond to Cu(0) and Cu(I). The latter seems to be formed during surface preparation prior to electrodeposition. The Cu $2p_{1/2}$ peak at 935.23 is also present. Table IV summarizes the characteristics of the Cu $2p_{3/2}$ peaks obtained from the XPS spectrum.

Figure S1e (Supporting Information) shows the XPS O 1s peaks. The O 1s band has a notable intensity at 532.00 eV from O(0). The two other peaks at 529.7 and 530.5 eV are related to CuO and Cu_2O, respectively. Table V presents the O content determined from the XPS peaks.

Topographic image of Sample 1 shown in Figure 2 indicates conical gold particles electrodeposited on the copper substrate at 50 Hz. Figure 2(b) illustrates the image of clustered AuNPs at higher magnification. As a general rule, a homogeneous distribution of Au particles with conical shape is observable on the entire AuNPs-Cu electrode.

Table IV. Substrate Cu Content Based on the XPS Peaks

	Cu $2p_{3/2}$		
Element	BE (eV)	FWHM	Rel. Area (Pct)
Cu	932.60	1.88	39.8
CuO	933.90	3.11	59.9
Cu_2O	932.40	1.91	0.3

Table V. Substrate O Content Based on the XPS Peaks

	O 1s		
Element	BE (eV)	FWHM	Rel. Area (Pct)
O	532.00	2.23	80.0
CuO	529.70	2.15	7.6
Cu_2O	530.5	1.62	12.4

B. *Effect of Frequency on the Surface Morphology of Deposit*

Effect of the applied pulse frequency on the surface morphology of the coatings is shown in Figure 3. From AFM images, the mean diameter of the gold nanoparticles electrodeposited on the Cu substrate is obtained, as indicated in Figure 3. The obtained values for Sample 1, 2, and 3 are 85 ± 10, 89 ± 28, and 29 ± 8 nm, respectively.

Increasing pulse frequency from 50 to 100 Hz does not have significant effect on the particle size of the deposit, while increasing the pulse frequency in a similar interval up to 142.8 Hz results in significantly smaller particle sizes than those obtained at 100 Hz.

Morphology of the AuNP layer depends on the deposition duration, the applied potential, the solution concentration, and the substrate preparation procedure.

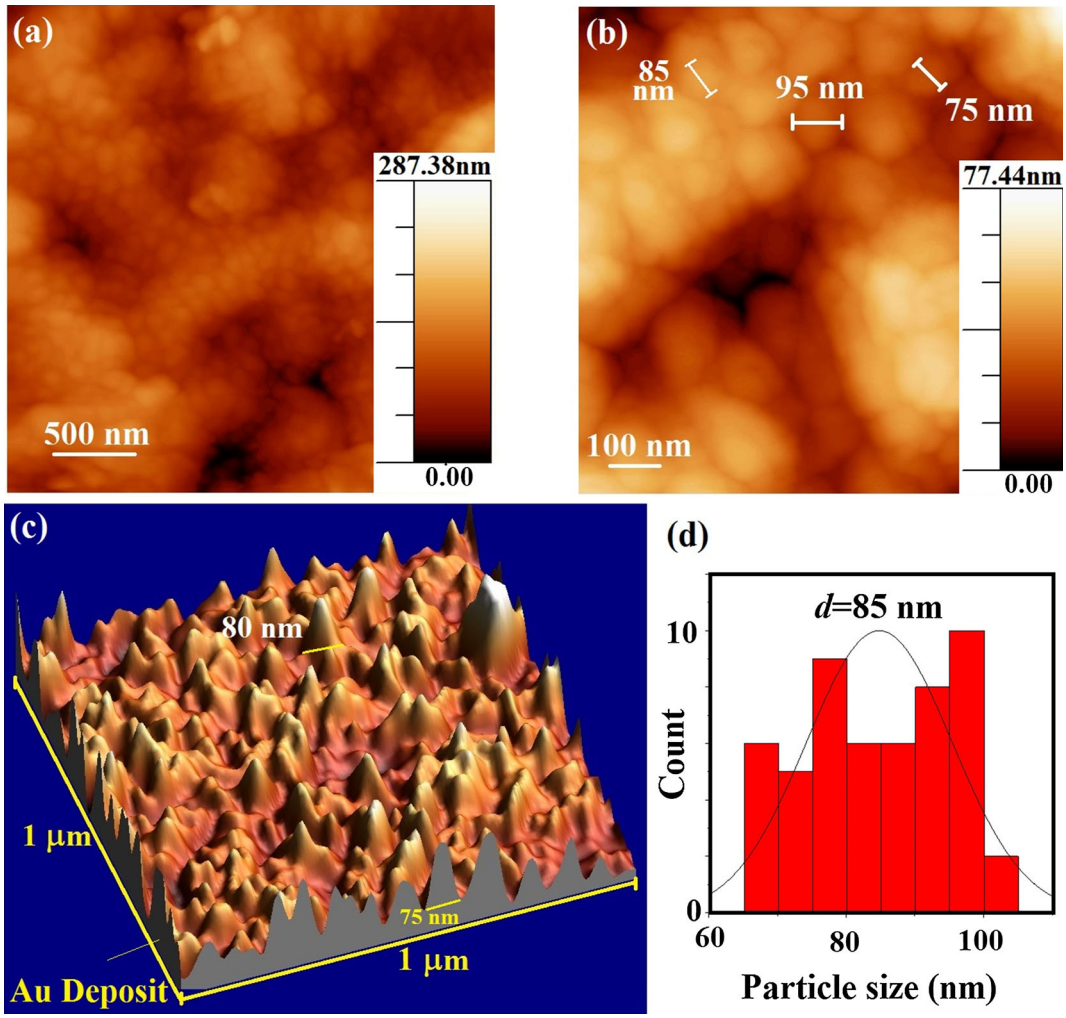

Fig. 2—AFM images of the particles electrodeposited on Cu electrode at 50 Hz: (*a*) 2D, (*b*) high magnification 2D, (*c*) 3D, and (*d*) particle size histogram.

Pulse frequency influences on metallic ions of the diffusion layer and the surface overpotential. According to the nucleation theory, it is expected to fine-grained deposits obtained at higher nucleation rates produced by diffusion layer vibrations created at large pulsation rates.

However, in pulse electrodeposition process, the electric double layer effect also occurs at the cathode/solution interface which represents a capacitor of molecular dimensions and stores the electrical energy.[28] Therefore, the total current i_{total} supplied by the generator consists of a capacitive current, C_{DL}, and a Faradaic current, i_{F}, as:

$$i_{\text{total}} = i_{\text{F}} + C_{\text{DL}} \frac{\mathrm{d}E}{\mathrm{d}t} \quad [9]$$

$$C_{\text{DL}} = \frac{\varepsilon}{\lambda(2\pi f)^{0.5}} \cosh \frac{zFE}{2RT}, \quad [10]$$

where E is the potential drop at the electrode surface, ε is the permittivity of the solution, λ is the Debye length based on surface concentrations and f is the pulse frequency.

Based on Eqs. [9] and [10], increasing the C_{DL} can lead to smaller i_{F} than i_{total}. Decreasing the Faradaic current causes the lower overpotential than expected.

According to Eq. [10], C_{DL} has an inverse square root dependence on pulse frequency. The previous studies[28] indicated that the effect of electric double layer capacitance is significant at low frequencies, but becomes very small at high frequencies.

Therefore, the insignificant change in particle size with increasing pulse frequency from 50 to 100 Hz may be due to electric double layer capacitance at low frequencies. While, increasing the frequency up to 142.8 Hz, size reduction of the deposited grains occurs as a result of decreasing the electric double layer effect.

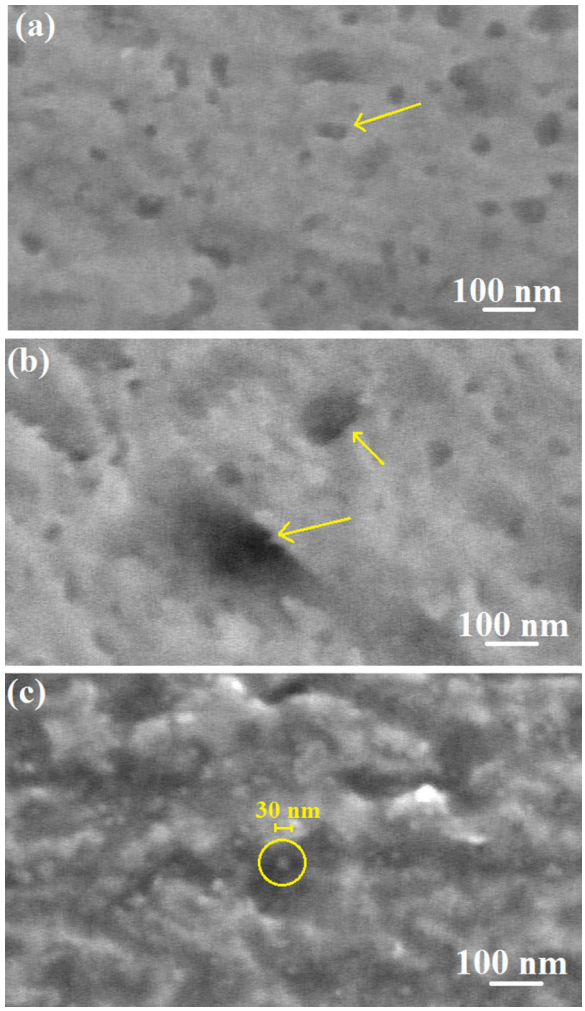

Fig. 4—FE-SEM images of the AuNPs-Cu electrodes at frequencies of (*a*) 50, (*b*) 100, and (*c*) 142.8 Hz. The arrows show porosities in (a) and (b) and the circle highlights a typical particle in (c).

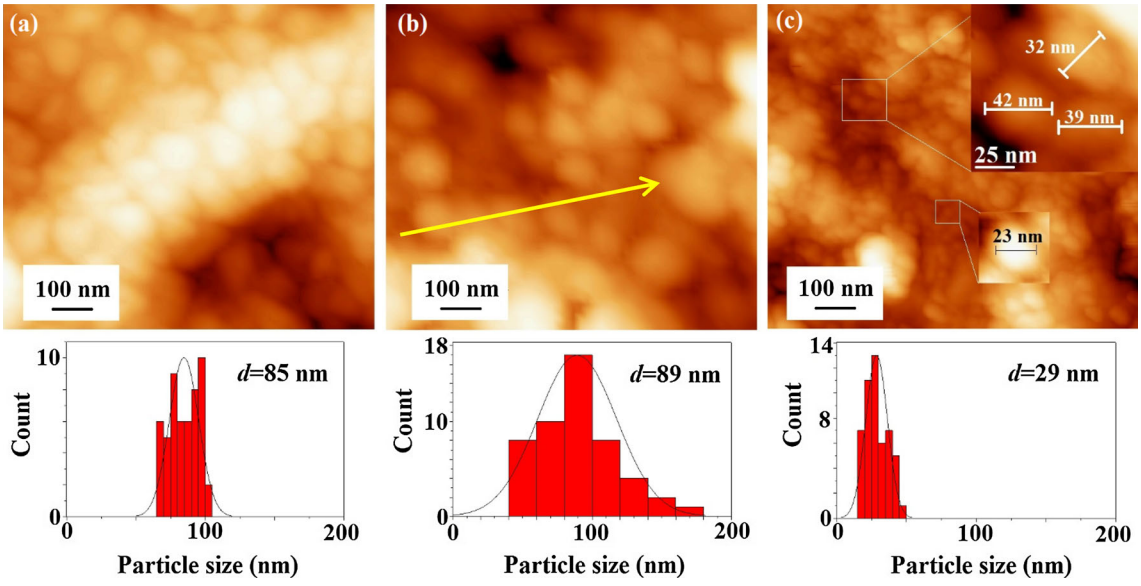

Fig. 3—AFM images of the AuNPs-Cu electrodes at frequencies of (*a*) 50, (*b*) 100, and (*c*) 142.8 Hz.

Table VI. Length and Area of the AuNPs-Cu Electrodes Porosity in Different Frequencies (Duty Cycle = 30 Pct, Current Density = 10 mA/cm^2, Real Time = 1 min with Cysteine Additive)

	Length (nm)				Area (nm^2)			
Frequency (Hz)	Minimum	Maximum	Mean	Sum	Minimum	Maximum	Mean	Sum
50	0.0337	100	60	13,200	703.3	7600	2100	500,000
100	0.0632	200	118	2800	2500	17,400	7800	200,000
142.8	0.0223	100	52	1300	360.2	6200	1500	38,400

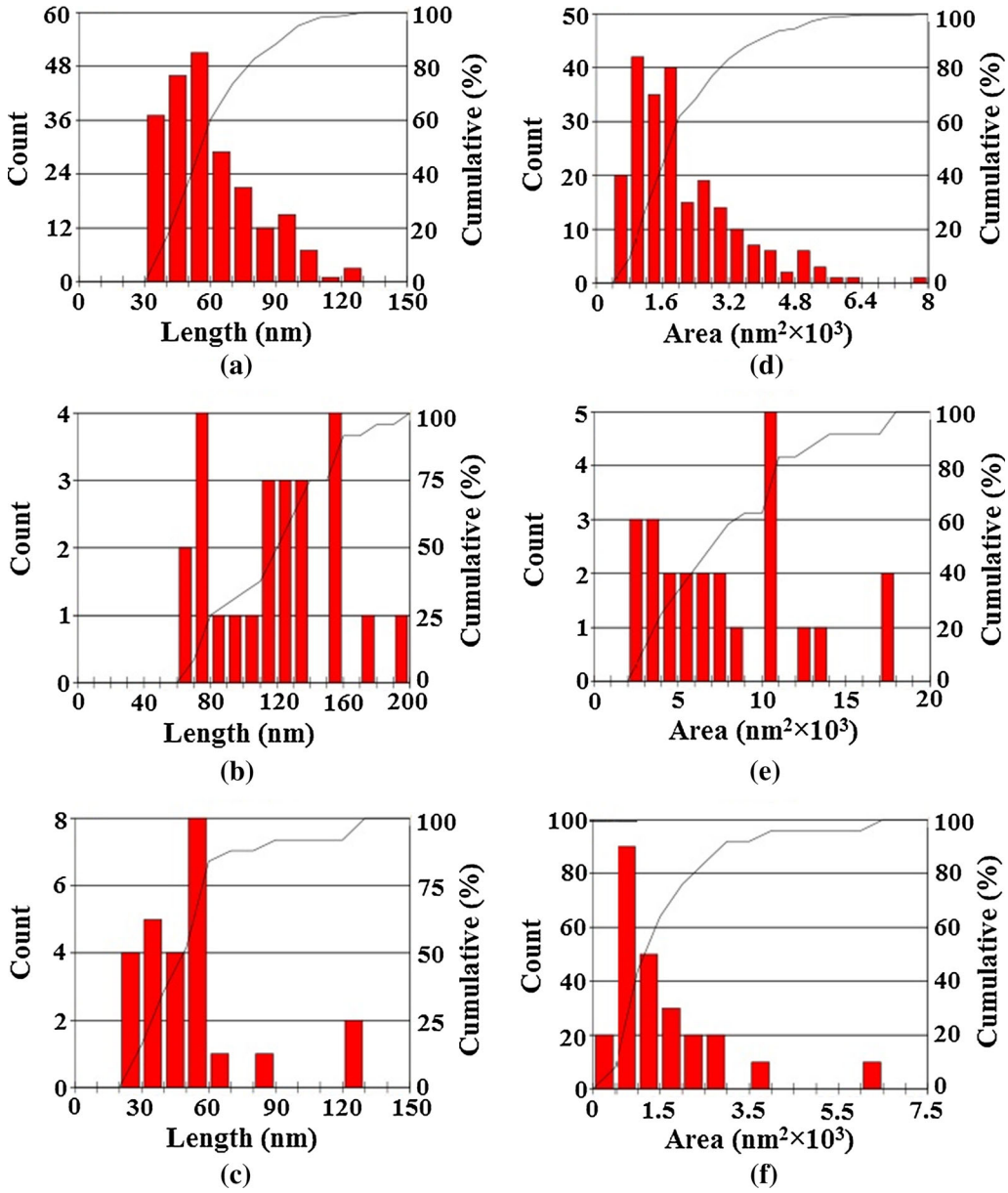

Fig. 5—Histograms and Cumulative (pct) line graph of the pore lengths (*a*, *b*, and *c*) and areas (*d*, *e*, and *f*) of AuNPs-Cu electrodes created at frequencies 50, 100, and 142.8 Hz, respectively, (Cumulative (pct) line graph, as shown by a black line in the histogram, represents the percentage of features that are below or above a given measurement value).

The influence of frequency on the morphologies of AuNPs electrodeposited on Cu electrode is also studied by FE-SEM observations (Figures 4(a) through (c)). Rise of the layer thickness near pores of the deposited film by pulse frequency is clearly observable in images (a) and (b) of Figure 4. This result is confirmed by current efficiency enhancements shown in Table III.

At lower frequencies, clusters easily split into sectors. Overlapping particles are hence observed at 50 and 100 Hz as illustrated in Figures 4(a) and (b). At

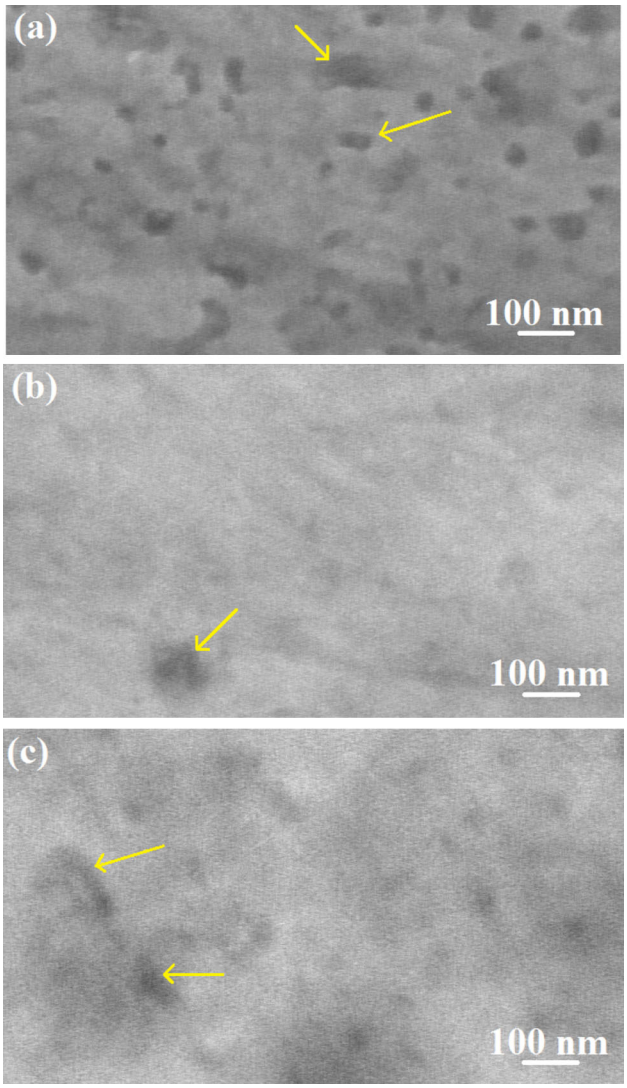

Fig. 6—FE-SEM images of the AuNPs-Cu electrodes at (*a*) 10, (*b*) 5, and (*c*) 2.5 mA/cm^2. (The bright and dark regions indicate the Au cover layer and Cu substrate, respectively. The arrows show porosities in the AuNPs-Cu electrodes).

142.8 Hz, large number of small AuNPs on the surface of the deposited layer is observed (Figures 3(c), 4(c)), which is consistent with the values obtained from AFM images for size of the particles (Figure 3(c)). Clustering causes particle size enhancement. At higher frequency of 142.8 Hz, the average AuNPs size is ~30 nm, as highlighted with the circle of Figrue 4(c). Porosity of the electrodeposited AuNPs-Cu electrodes determined from FE-SEM images indicates reducing effect of the frequency of the pulse current.

Length and area of the porosity indicate initial escalation (from 50 to 100 Hz) and subsequent diminution (from 100 to 142.8 Hz) with the pulse frequency (Table VI). Because of the lower lengths and areas (and their sum) at 142.8 Hz, a better surface quality is obtained at this frequency. Histograms plotted in Figure 5 shows pore characteristics of the Samples 1, 2, and 3.

C. *Effect of Current Density on the Surface Morphology of Deposit*

Effect of current density on morphology of the AuNPs deposit is shown in Figures 6 and 7. As is observable in Figure 6, decrease of current density significantly lowers the porosity of the layer. According to Table III, by decreasing the current density form 10 to 5 mA/cm^2, the current efficiency increases and then decreases from 5 to 2.5 mA/cm^2. It is evident from Figure 7 that the size of particles decreases from 85 nm (SD = 10 nm) to 32 nm (SD = 7 nm) by decreasing the applied current density from 10 to 5 mA/cm^2, whereas the decrease of current density from 5 to 2.5 mA/cm^2 leads to a rise in particle size from 32 nm (SD = 7 nm) to 108 nm (SD = 24 nm). According to the experimental observations, nucleation density exponentially increases with the overpotential of the pulsating system. The exponential dependence is due to activation energy distribution close to the diffusion layer adjacent to the nucleation locations.[5] As a result, the particle size decreases when the current density enhances from 2.5 to 5 mA/cm^2. However, the current density increase from 5 to 10 mA/cm^2 can lead to a decreased overpotential which has been reported in previous studies[29] as a contrary behavior to theoretical studies. As a result, particle size growth occurs which favored at low overpotential.[30] This result is consistent with the previous report that has shown complex relationship between current and electric potential.[29]

D. *Effect of Additive on the Surface Morphology of Deposit*

Effect of cysteine and potassium iodide additives on morphology of the AuNPs electrodeposited on Cu layer is shown in Figure 8. According to the figure, iodide ion causes reduction of porosity and rising of nanoparticles number. Two particles are highlighted with arrows in the figure. In presence of the iodide ions, the particles deposited on the Cu substrate become smaller than 50 nm.

Presence of cysteine or iodide ions in the electrochemical solution has the following substantial effects on the AuNPs deposited layer: (1) change in size of the gold nanoparticle and (2) variation of particles orientation.[31] Initial-stage nucleation-growth kinetics of the electrodeposition depends on the solution composition, pH, temperature, substrate material, and physical and morphological properties of the deposited layer.[32] Previous researchers have reported in the presence of 100 μM cysteine and iodide ions that cause the AuNPs to enrich along (100) and (110) orientations with particle sizes of 50 to 300 nm and (111) with particle sizes ranging from 10 to 40 nm, respectively.[31] Particle size reduction from about 90 to 50 nm is also occurred in present study by changing the cysteine to iodide ions as additives, which consistent with results of previous investigation.[31]

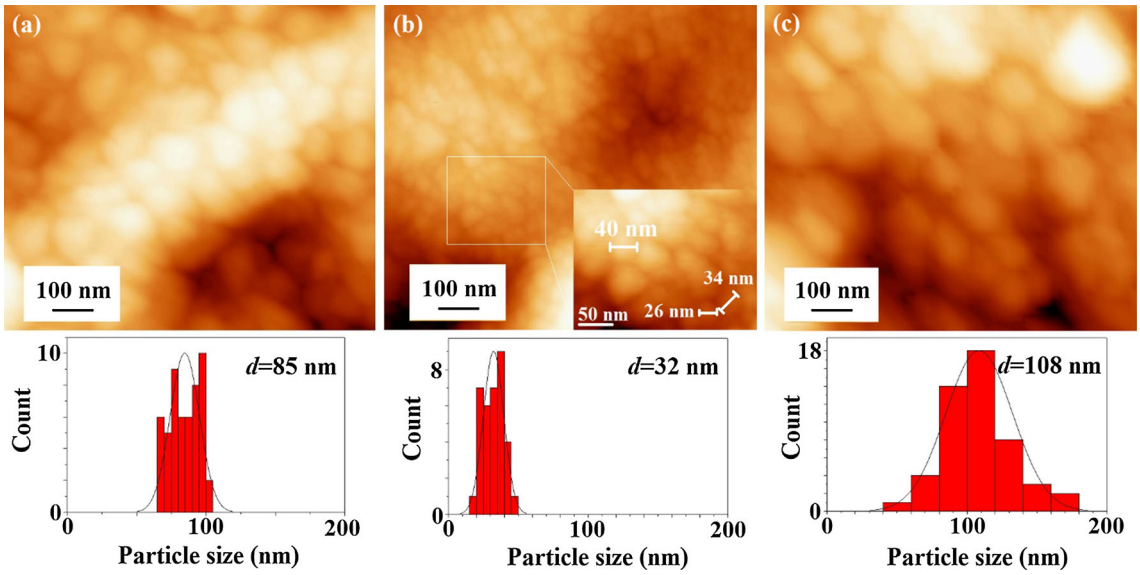

Fig. 7—AFM images of the AuNPs-Cu electrodes at frequencies at (*a*) 10, (*b*) 5, and (*c*) 2.5 mA/cm^2.

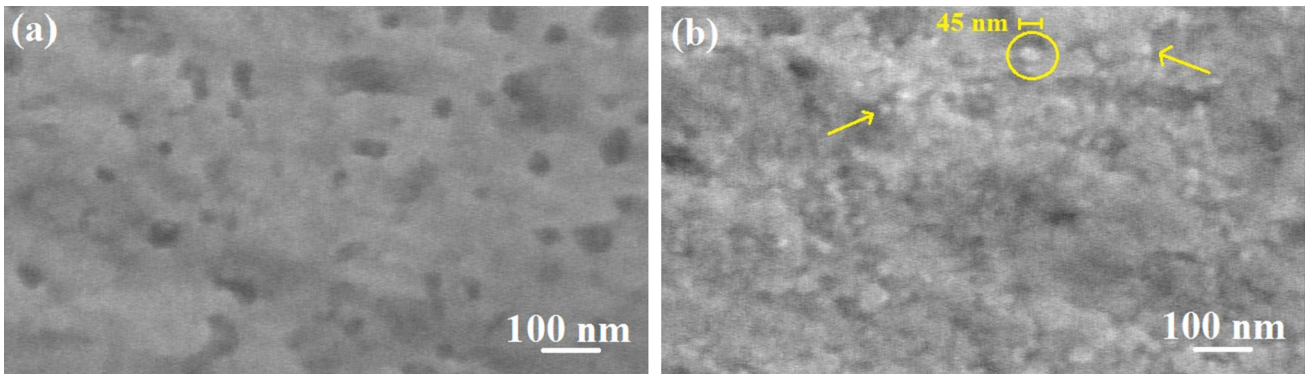

Fig. 8—FE-SEM images of the AuNPs-Cu electrodes in the presence of (*a*) cysteine and (*b*) potassium iodide additives.

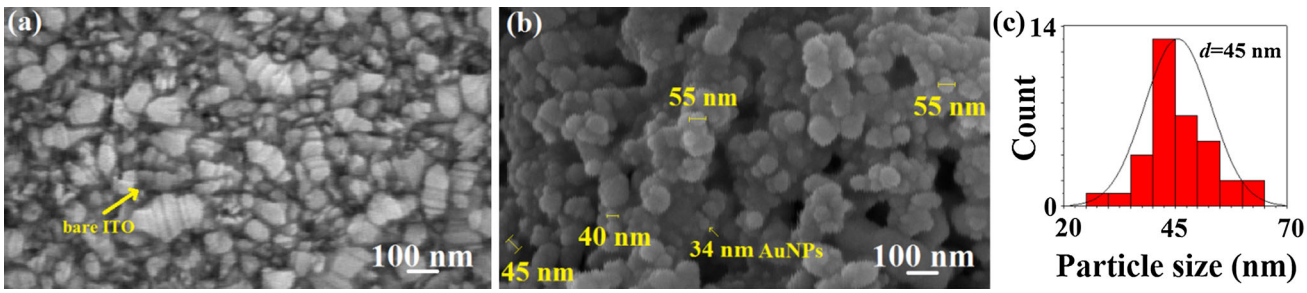

Fig. 9—FE-SEM image of the (*a*) bare ITO, (*b*) AuNPs-ITO electrode, and (*c*) particle size histogram of AuNPs electrodeposited on the ITO electrode. The substrate is completely covered with AuNPs.

E. *Effect of Substrate Type on the Surface Morphology of Deposit*

For deposit thicknesses equal or greater than 1 μm, morphology principally depends on the electrochemical parameters. Deposit thickness decreases, however, with nature of the deposition substrate.[33] Theoretical thickness of the deposit in all samples (except Sample 5) is 0.2 μm. This value for Sample 5 is 0.05 μm. The nature of the substrate plays, hence, a critical role in the surface morphology of the deposited layer.

According to Figure 9, the average size of the electrodeposited AuNPs is 45 nm (SD = 7 nm), while the mean particle diameter of the film deposited on Cu electrode (as shown in Figure 3) is 85 nm (SD = 10 nm). Based on the previous investigations,[34] the substrate electrical resistance has reverse particle size dependence. Since ITO has higher electrical resistance than Cu, lower size AuNPs grow on the ITO electrode. Histograms of the AuNPs formed on the ITO electrode are shown in Figure 9(c).

IV. CONCLUSIONS

Highly conductive AuNPs-Cu and AuNPs-ITO cathodes were produced by pulse-current electrodeposition of nanoparticles on Cu and coated glasses. Effects of PED parameters, current density, electric frequency, and cysteine/iodide ions presence on current efficiency, morphology, and porosity of the produced layers were investigated. XPS studies revealed that appropriate surface quality with no AuCN adsorption could occur at 10 mA/cm^2. Results showed that porosity of the layer decreases with escalation of the current frequency to 142.8 Hz, diminution of the current density to 2.5 mA/cm^2 and addition of potassium iodide to the electrolyte solution. They also revealed that the thickness of the deposited layer and the cathode current efficiency increase with the current frequency, the iodide ion presence and the AuNPs deposition on the Cu layer. They increased with decreasing the current density from 10 to 5 mA/cm^2 and decreased, however, with lessening of the current density to 2.5 mA/cm^2. Current efficiency improvement and AuNPs size reduction (to 50 nm) occurred with increasing of the frequency and addition of the iodide ion. Alternative ITO substrate resulted in nucleation sites multiplication, surface morphology improvement, particle-number escalation, and grain size variation for AuNPs grown on the cathode sample.

ACKNOWLEDGMENTS

The authors would like to acknowledge R. Siavash Moakhar for assistance with fabrication of AuNPs-ITO electrodes.

ELECTRONIC SUPPLEMENTARY MATERIAL

The online version of this article (doi:10.1007/s11663-015-0427-6) contains supplementary material, which is available to authorized users.

REFERENCES

1. R.K. Sarvestani and J.D. Williams: *Electrochem. Solid State*, 2010, vol. 13, pp. D37–39.
2. X. Dai and R.G. Compton: *Anal. Sci.*, 2006, vol. 22, pp. 567–70.
3. B. Ballarin, M.C. Cassani, C. Maccato, and A. Gasparotto: *Nanotechnology*, 2011, vol. 22, p. 275711.
4. M. Oyama: *Rev. Polarogr.*, 2007, vol. 53, pp. 3–18.
5. T.S. Olson, P. Atanassov, and D.A. Brevnov: *J. Phys. Chem. B*, 2004, vol. 109, pp. 1243–50.
6. D. Mei Gao, Y.Y. Sun, Q. Zhao, J. Bo Hu, and Q. Long Li: *Microchim. Acta*, 2008, vol. 160, pp. 241–46.
7. Y.-Y. Tang and P.-Y. Chen: *J. Chin. Chem. Soc-Taip.*, 2011, vol. 58, pp. 723–31.
8. L. Wang, W. Mao, D. Ni, J. Di, Y. Wu, and Y. Tu: *Electrochem. Commun.*, 2008, vol. 10, pp. 673–76.
9. N. Sakai, Y. Fujiwara, M. Arai, K. Yu, and T. Tatsuma: *J. Electroanal. Chem.*, 2009, vol. 628, pp. 7–15.
10. J. Zhang, M. Kambayashi, and M. Oyama: *Electroanalysis*, 2005, vol. 17, pp. 408–16.
11. J. Zhang and M. Oyama: *Anal. Chim. Acta*, 2005, vol. 540, pp. 299–306.
12. J. Zhang and M. Oyama: *Electrochim. Acta*, 2004, vol. 50, pp. 85–90.
13. J. Zhang and M. Oyama: *J. Electroanal. Chem.*, 2005, vol. 577, pp. 273–79.
14. J. Zhang and M. Oyama: *Electrochem. Commun.*, 2007, vol. 9, pp. 459–64.
15. A.A. Umar and M. Oyama: *Indian J. Chem. Inorg. Phys. Theor. Anal. Chem.*, 2005, vol. 44, pp. 938–44.
16. R.N. Goyal, M. Oyama, and A. Tyagi: *Anal. Chim. Acta*, 2007, vol. 581, pp. 32–36.
17. F.D. Barlow and A. Elshabini: *Ceramic Interconnect Technology Handbook*, CRC Press, Boca Raton, 2005, p. 328.
18. T.-H. Kao, J.-M. Song, I.-G. Chen, T.-Y. Dong, and W.-S. Hwang: *Nanotechnology*, 2007, vol. 18, p. 435708.
19. I. Kityk, K. Plucinski, J. Ebothé, A.A. Umar, and M. Oyama: *J. Appl. Phys.*, 2005, vol. 98, pp. 1–4.
20. F. Sun, W. Cai, Y. Li, G. Duan, W.T. Nichols, C. Liang, N. Koshizaki, Q. Fang, and I.W. Boyd: *Appl. Phys. B*, 2005, vol. 81, pp. 765–68.
21. J. Ustarroz, U. Gupta, A. Hubin, S. Bals, and H. Terryn: *Electrochem. Commun.*, 2010, vol. 12, pp. 1706–09.
22. M.-C. Tsai and P.-Y. Chen: *Talanta*, 2008, vol. 76, pp. 533–39.
23. A. Dolati, I. Imanieh, F. Salehi, and M. Farahani: *Mater. Sci. Eng. B*, 2011, vol. 176, pp. 1307–12.
24. Y. Qi-Xia: *Plat. Surf. Finish.*, 1989, vol. 76, pp. 52–53.
25. B. Bozzini, C. Mele, and V. Romanello: *J. Electroanal. Chem.*, 2006, vol. 592, pp. 25–30.
26. D.M. Mac Arthur: *J. Electrochem. Soc.*, 1972, vol. 119, pp. 672–77.
27. P.A. Kohl: in *Modern Electroplating*, M. Schlesinger and M. Paunovic, eds., Wiley, New York, 2010, p. 115.
28. N. Tantavichet and M.D. Pritzker: *J. Electrochem. Soc.*, 2002, vol. 149, pp. C289–99.
29. F. Ebrahimi and Z. Ahmed: *J. Appl. Electrochem.*, 2003, vol. 33, pp. 733–39.
30. A.F. Zimmerman, D.G. Clark, K.T. Aust, and U. Erb: *Mater. Lett.*, 2002, vol. 52, pp. 85–90.
31. M.S. El-Deab, T. Sotomura, and T. Ohsaka: *Electrochem. Commun.*, 2005, vol. 7, pp. 29–34.
32. Y. Li, W. Chrzanowski, and A. Lasia: *J. Appl. Electrochem.*, 1996, vol. 26, pp. 843–52.
33. M. Paunovic, M. Schlesinger, and D.D. Snyder: *Modern Electroplating*, M. Schlesinger and M. Paunovic, eds., Wiley, New York, 2010, p. 1.
34. A. Bouraiou, M. Aida, E. Tomasella, and N. Attaf: *J. Mater. Sci.*, 2009, vol. 44, pp. 1241–44.